

Circular Dielectric Rod With Conformal Strip of Graphene as Tunable Terahertz Antenna: Interplay of Inverse Electromagnetic Jet, Whispering Gallery and Plasmon Effects

Sergii V. Dukhopelnykov ¹, *Member, IEEE*, Mario Lucido ², *Senior Member, IEEE*,
Ronan Sauleau ³, *Fellow, IEEE*, and Alexander I. Nosich ⁴, *Fellow, IEEE*

Abstract—In this article, we consider the radiation characteristics of a THz antenna made of a circular dielectric rod decorated with conformal graphene strip and illuminated by the field of a line magnetic current. The strip has arbitrary angular size and location and its surface impedance is characterized with Kubo theory. Our mathematically accurate analysis uses a dedicated hypersingular integral equation for the current induced on the strip. Discretization of this equation is carried out by the Nystrom-type method, which has a guaranteed convergence. We study the dependences of the powers radiated and absorbed in this configuration and also the directivity of antenna emission, in wide frequency range from 0 to 10 THz. They show very interesting interplay between the broadband inverse photonic-jet effect of lens-like dielectric rod and two types of resonances: on the moderate-Q plasmon modes of graphene strip and on the extremely high-Q whispering-gallery modes of the circular rod.

Index Terms—Circular dielectric rod, graphene strip, line current, integral equation, plasmon, inverse photonic jet.

I. INTRODUCTION

BOTH in THz and shorter frequency ranges, a ubiquitous element of almost every sensor is an integrated lens antenna, which concentrates the incoming electro-magnetic waves on a miniature receiving circuit. Perhaps, the simplest design of a lens is a uniform optically transparent sphere or, in two-dimensional (2-D) case, circular cylinder, or rod. This is because such a sphere or a rod produces a remarkable near-field phenomenon, which at first obtained the name “nanojet” and later became known as “photonic jet” [1], [2]. In fact, it should be, probably,

Manuscript received March 30, 2020; revised August 27, 2020; accepted September 1, 2020. Date of publication September 10, 2020; date of current version October 8, 2020. This work was supported in part by the National Research Foundation of Ukraine under Project 2020.02.0150. (*Corresponding author: Sergii V. Dukhopelnykov.*)

Sergii V. Dukhopelnykov and Alexander I. Nosich are with the Laboratory of Micro and Nano Optics, Institute of Radio-Physics and Electronics NASU, 61085 Kharkiv, Ukraine (e-mail: dukh.sergiy@gmail.com; anosich@yahoo.com).

Mario Lucido is with the DIEI, University of Cassino and Southern Lazio, 03043 Cassino, Italy (e-mail: lucido@unicas.it).

Ronan Sauleau is with the IETR, Universit  de Rennes 1, 35042 Rennes, France (e-mail: ronan.sauleau@univ-rennes1.fr).

Color versions of one or more of the figures in this article are available online at <https://ieeexplore.ieee.org>.

Digital Object Identifier 10.1109/JSTQE.2020.3022420

called “electromagnetic jet” (EMJ), because this phenomenon can be found in all frequency ranges, if only the relative dielectric permittivity of sphere or rod is $\varepsilon < 4$ and its radius is $R \geq 2\lambda$, where λ is the free-space wavelength [1], [2]. If the radius gets larger, EMJ becomes more intensive and concentrated. This is, in fact, a phenomenon of imperfect near-field focusing, which can be explained, in essence, using the geometrical optics (GO). Hence, it is broadband and, in the 2-D case, takes place both in the E-polarization case (electric field is parallel to the rod) and the H-polarization one (magnetic field is parallel to the rod). Note that the focusing can be enhanced greatly by making the sphere or rod discrete, i.e. made of concentric layers, with their dielectric constants mimicking the Luneburg lens [3], [4].

According to the reciprocity theorem of classical electromagnetics, if a point source is placed into EMJ area then, in the far zone, a sharp lobe of the angular radiation pattern appears. This far-field collimation can be also called “inverse EMJ” effect; in 2-D, it was studied in [5].

Besides of the GO effects, any finite-size dielectric object is an open resonator, which possesses a discrete spectrum of natural modes. The Pointing theorem tells that such mode frequencies can be only complex valued, i.e. the associated Q-factors are always finite, because of the radiation losses. Out of all dielectric objects, those, which are circular at least in some cross-section, stand out, supporting the whispering-gallery (WG) modes. In ideal sphere and circular rod, WG modes have Q-factors, exponentially growing up with radius, or mode index, that kills performance of rough commercial codes [6]–[8]. Note that both EMJ and inverse-EMJ effects on finite-radius rod are spoiled by the “ignition” of a WG mode because its near field starts dominating over the GO field [5].

Today, nanotechnologies open new opportunities in the design of many optical and photonics devices, and frequently this is connected to the use of graphene. Besides of the DC tunability of its electron conductivity defined by the chemical potential, frequency, temperature, and relaxation time, a major feature of micro and nanosize graphene samples is their ability to support plasmon modes in the THz to infrared ranges [9], [10]. Both flat and curved graphene strips attract attention today as easily fabricated tunable components of plasmonic antennas, waveguides, and sensors [11]–[15]. Recently, in [16] it was shown that

a resonance graphene strip placed into the EMJ area of a circular dielectric rod enhances greatly the near field without increasing the rod radius or refractive index.

Guided by the reciprocity principle, in this work we consider the radiation a THz range line magnetic current in the presence of a circular dielectric rod, decorated with a conformal strip of graphene. Our aim is to study the inverse-EMJ effect, i.e. the far-field directivity enhancement and how can it be controlled with the aid of graphene strip. In our analysis, we combine the Maxwell boundary-value problem with the Kubo conductivity of graphene, considered as a zero-thickness layer with complex surface impedance [9].

As it was pointed out to earlier [17], [18], such a study is equivalent to accurate quantification of the Purcell effect, i.e. the modification of the power, radiated by a point source (in 2-D) in the presence of composite open cavity: dielectric rod with graphene strip. Note that description of this effect with the aid of a simplified quantity called ‘‘Purcell factor’’ [18] is not accurate and should be replaced with numerical analysis.

As circular rod is a simple shape, the center of gravity of a trusted numerical technique is associated with consideration of the graphene strip. Commercial code treatments of zero-thickness strip meet certain difficulties (see Introduction in [19]), however, several convergent methods, developed earlier to study the scattering from perfectly electrically conducting (PEC) strips are available. Among them, we have two analytical regularization techniques: regularizing method-of-moments and Riemann-Hilbert Problem (RHP) method, and a Nystrom-type discretization with Chebyshev quadratures [19]–[21]. The use of these mathematically justified methods allows solving the considered problems quickly and with controlled accuracy even in the sharp WG-mode resonances.

Important examples of such analyses cover flat graphene strip scattering in [12], [14]. Plasmon-mode resonances in the scattering and absorption by the gratings of coplanar graphene strips were analyzed in [19]–[21]. The accurately studied curved graphene configurations are restricted to fully covered circular dielectric rod [22]–[24] and parabolic reflector in air [25].

In our analysis, we use the technique of [16], extensively validated there and adapted here to the line current excitation.

II. MATHEMATICAL MODEL

Consider a cylindrical time-harmonic ($e^{-i\omega t}$) wave emitted by a magnetic-line current located near to a circular dielectric rod, the outer boundary of which is partially covered with conformal strip of graphene. The cross section of such antenna configuration by the coordinate plane $z = 0$ is presented in Fig. 1. Here, R is the radius of the rod, 2δ is the angular width of the graphene strip, $2\theta = 2\pi - 2\delta$ is the angular width of the slot, and D_s is the distance from the source to the rod. The electromagnetic field is H-polarized.

Considering the case of H_z field not depending on z , we obtain the following 2-D problem. Find the function $H_z(r, \phi)$, which satisfies (i) the Helmholtz equation with the wavenumber k^I , or k^{II} for all $r \neq R$, (ii) the dual boundary condition at $r = R$: on

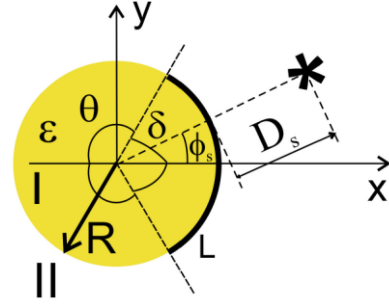


Fig. 1. Cross-section of a dielectric rod with a conformal graphene strip illuminated by a magnetic line current.

the strip arc, $L : \{r = R, |\phi - \phi_0| \leq \delta\}$,

$$E_\phi^I + E_\phi^{II} = 2ZZ_0(H_z^I - H_z^{II}), E_\phi^I = E_\phi^{II}, \quad (1)$$

and on the slot arc, $S : \{r = R, |\phi - \phi_0| \leq \theta\}$,

$$H_z^I = H_z^{II}, E_\phi^I = E_\phi^{II} \quad (2)$$

(iii) the Sommerfeld radiation condition at infinity, and (iv) the local power finiteness condition (a.k.a. edge condition).

Here, $ZZ_0 = 1/\sigma$ is the graphene surface impedance, σ is the surface conductivity, Z_0 is the impedance of the free space, index $I(II)$ is assigned to the inside (outside) domain filled with nonmagnetic material having permittivity $\varepsilon_I(\varepsilon_{II})$, and $k_{I,II} = (\omega/c)\sqrt{\varepsilon_{I,II}}$, where c is the speed of light.

The incident cylindrical wave, $H_z^{inc} = H_0^{(1)}(k^I|\vec{r} - \vec{r}_s|)$, is emitted by the magnetic line current, placed at the point \vec{r}_s .

$$\begin{aligned} & H_0(k|\vec{r} - \vec{r}_s|) \\ &= \begin{cases} \sum_{n=-\infty}^{+\infty} J_n(kr)H_n(kr_s)e^{in(\phi-\phi_s)}, & R < r < r_s, \\ \sum_{n=-\infty}^{+\infty} J_n(kr_s)H_n(kr)e^{in(\phi-\phi_s)}, & r > r_s, \end{cases} \quad (3) \end{aligned}$$

The total field can be presented as the Fourier series

$$H_z^{(I,II)} = \begin{cases} \sum_{n=-\infty}^{+\infty} C_{1,n}J_n(k^I r) e^{in\varphi}/d_n, & r < R, \\ H_z^{inc} + \sum_{n=-\infty}^{+\infty} C_{2,n}H_n(k^{II} r) e^{in\varphi}/h_n, & r \geq R, \end{cases} \quad (4)$$

Here, $d_n = J'_n(k^I R)$, $h_n = H'_n(k^{II} R)$, $J_n(\cdot)$ and $H_n(\cdot)$ are the Bessel and Hankel first kind functions, the prime means differentiation in argument, and $C_{(1,2),n}$ are unknown coefficients, which should be found. Such a field satisfies the Helmholtz equation and the radiation condition.

Following [16], we derive a dual series equation for the unknown coefficients x_q , linearly related to $C_{(1,2),q}$. Using the parametric representations [26] of the integral operators with hyper-singular and logarithmic kernels, we reduce it to a boundary hyper-singular integral equation. Applying a Nystrom-type method with the Chebyshev quadratures, we discretize that equation as follows:

$$x_q + \sum_{p=1}^N A_{qp}x_p = b_q, \quad q = 1, \dots, N, \quad (5)$$

where $b_q = -f(t_{0q})/Z_q$ are known, $Z_q = i\delta Z(1 - t_{0q}^2)$, and the elements of the matrix take the form,

$$A_{qq} = Z_q^{-1} \left\{ -\frac{1}{2}B_1(N+1)^2 - B_2\delta^2 \left[1 - (t_{0q})^2 \right] \right\}$$

$$\times \left[\ln 2 + 2 \sum_{s=1}^N T_s(t_{0q})T_s(t_{0q})/s + (-1)^{2q}/(2N+2) \right] - 2\delta^2(1-t_{0q}^2)K(t_{0q}, t_{0q}) \} / (N+1), \quad (6)$$

$$A_{qp} = Z_q^{-1} \left\{ B_1 \left[1 - (t_{0p})^2 \right] \frac{1 - (-1)^{q+p}}{(t_{0q} - t_{0p})^2} - B_2 \delta^2 \left[1 - (t_{0p})^2 \right] \times \left[\ln 2 + 2 \sum_{s=1}^N T_s(t_{0p})T_s(t_{0q})/s + (-1)^{p+q}/(2N+2) \right] - 2\delta^2 \left[1 - (t_{0p})^2 \right] K(t_{0q}, t_{0p}) \right\} / (N+1), \quad (7)$$

Using (3), the right part can be written as follows:

$$f(\phi) = \sum_{n=-\infty}^{\infty} J'_n H_n(kr_s) H_n(H'_n)^{-1} W_n e^{-in\phi_s} e^{in\phi} - \sum_{n=-\infty}^{\infty} J_n H_n(kr_s) W_n e^{-in\phi_s} e^{in\phi} \quad (8)$$

where the omitted arguments of Bessel and Hankel functions are, respectively, $k^I R$ and $k^{II} R$, and other quantities are

$$K(t, t_0) = \sum_{n=1}^{\infty} (W_n - B_1 |n| - B_2 |n|^{-1}) \cos n(\theta - \pi)(t - t_0), \quad (9)$$

$$W_n = \left[\sqrt{\varepsilon_I} J_n(J'_n)^{-1} - \sqrt{\varepsilon_{II}} H_n(H'_n)^{-1} \right]^{-1}, \quad (10)$$

$$B_1 = 1/kR(\varepsilon_I + \varepsilon_{II}), \quad B_2 = -\frac{1}{2}kR(\varepsilon_I^2 + \varepsilon_{II}^2)(\varepsilon_I + \varepsilon_{II})^{-2} \quad (11)$$

Besides, $T_s(t_{0q})$ is Chebyshev polynomial of the first kind, and t_{0q} is zero of Chebyshev polynomial of the second kind.

The matrix equation (5) has strict diagonal predominance. The convergence of solution of (5) with $N \rightarrow \infty$ is guaranteed by the theorems of approximation of hyper-singular operators with the aid of quadratures [27], [28].

Further we compute and discuss several characteristics, which depend on the frequency and size of the graphene strip. In the far zone, the total field is a cylindrical wave

$$H_z(\vec{r}) = \Phi(\phi)(1/i\pi kr)^{1/2} e^{ikr} \quad (12)$$

with the following parts of the angular radiation pattern,

$$\Phi(\phi) = \Phi_{in}(\phi) + \Phi_{sc}(\phi), \quad \Phi_{in}(\phi) = e^{ikr_0 \cos(\phi - \phi_0)}, \quad (13)$$

$$\Phi_{sc}(\phi) = \sum_{n=-\infty}^{+\infty} (-i)^n h_n^{-1} C_{2,n} e^{in\phi} \quad (14)$$

The total radiation power is, by definition,

$$P_{rad} = (\pi k Z_0)^{-1} \int_0^{2\pi} |\Phi(\phi)|^2 d\phi \quad (15)$$

and then the substitution of (13) and (14) leads to

$$P_{rad}/P_0 = 1 + \sum_{n=-\infty}^{+\infty} \left[|y_n|^2 + 2\text{Re}(y_n^* J_n(kr_s) e^{-in\phi_s}) \right], \quad (16)$$

where $y_n = (-i)^n h_n^{-1} C_{2,n}$ and the normalization constant is the radiation power of the line in free space, $P_0 = 2(kZ_0)^{-1}$.

The absorption power consists of two parts, corresponding to the power, absorbed in the lossy graphene strip,

$$P_{abs}^{grph} = \text{Re} Z R \int_{-\delta}^{+\delta} |v(\phi)|^2 d\phi \quad (17)$$

and the power absorbed in the lossy dielectric rod,

$$P_{abs}^{diel} = 2\pi R |\varepsilon_I|^{-1} \sum_{m=-\infty}^{\infty} |C_{1,m}|^2 \text{Im} [\sqrt{\varepsilon_I} J_m(k^I R) J'_m(k^{II} R)] \quad (18)$$

Thus, the radiation efficiency (the quantum yield efficiency in the language of the Purcell effect) is the ratio,

$$\eta = P_{rad} / (P_{rad} + P_{abs}^{grph} + P_{abs}^{diel}) \quad (19)$$

The far-field directivity is the ratio of the power, radiated in the main-lobe direction, ϕ_{\max} , to the total radiated power,

$$D = 2(kZ_0 P_{rad})^{-1} |\Phi(\phi_{\max})|^2, \quad (20)$$

Note that the line-current directivity in the free space is 1.

Important part of the modeling is the description of the surface impedance of graphene. We use the Kubo formalism [9], according to which the graphene surface impedance, up to the visible-light frequencies, is given by

$$Z(\omega) \approx (Z_0 \sigma_{\text{intra}})^{-1} = (1/\tau - i\omega) / (Z_0 c_1), \quad (21)$$

where

$$c_1 = q_e^2 k_B T (\pi \hbar^2)^{-1} \times \left\{ \mu_c (k_B T)^{-1} + 2 \ln \left(1 + \exp(-\mu_c (k_B T)^{-1}) \right) \right\},$$

q_e is the electron charge, k_B is the Boltzman constant, T is the temperature, \hbar is the reduced Planck constant, τ is the electron relaxation time and μ_c is the chemical potential.

As known, a strip of graphene can be considered as a plasmon surface wave Fabry-Perot resonator [12], [16], [21]. If $|Z| \gg 1$, and neglecting the strip curvature, the approximate empiric equation for the plasmon modes is obtained as

$$\sin(\text{Re} \gamma_{plas} 2\delta R + \psi) \approx 0, \quad (22)$$

$$\gamma_{plas} \approx k [(\varepsilon_I + \varepsilon_{II})/2]^{1/2} [1 - Z^2(\varepsilon_I + \varepsilon_{II}) + O(Z^{-2})] \quad (23)$$

Here, ψ is the phase of the coefficient of reflection of the plasmon wave from the strip edge; the best fit is $\psi = \pi/4$.

The roots of (22) determine the natural frequencies of the plasmon modes P_m , whose fields are symmetric ($m = 1, 3, \dots$) and anti-symmetric ($m = 2, 4, \dots$) w.r.t. the strip middle point,

$$\omega_m^2 \approx \frac{1}{2} (\pi m - \psi) Z_0 c c_1 [(\varepsilon_I + \varepsilon_{II}) \delta R]^{-1} + O(Z^{-2}). \quad (24)$$

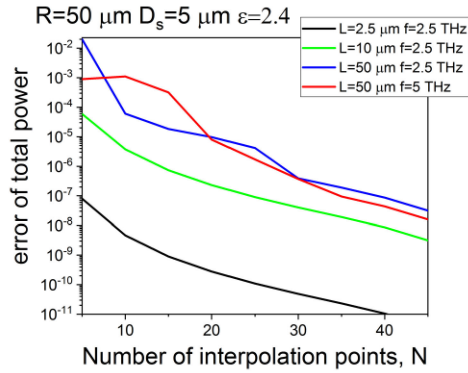


Fig. 2. Far-field computation error as a function of the order of interpolation in the Nystrom type discretization.

III. NUMERICAL RESULTS

First of all, to check the convergence we compute the error,

$$e_P(N) = |P_{rad}(N) - P_{rad}(N_{max})| / P_{rad}(N_{max}) \quad (25)$$

in the far-field power, as a function of the discretization order, with respect to the power computed at $N_{max} = 50$. These plots are presented in Fig. 2 and serve as the code validation. The antenna parameters are explained in the inset.

At first, we assume that the rod is lossless and $P_{abs}^{diel} = 0$. In Figs. 3 to 5, we present the spectral dependences, up to 10 THz, of (a) radiation power, (b) absorption power, and (c) directivity and the angle of the main lobe, ϕ_{max} (dotted lines).

The parameters of graphene and dielectric are the same for all figures: $\tau = 1$ ps, $T = 300$ K, $\mu_c = 0.5$ eV, and $\varepsilon = 2.4$. The source coordinates are taken on the x -axis all times.

In Figs. 3 and 4, the rod radius is $R = 50 \mu\text{m}$ and the strip width, $L = \delta R$, is different, $10 \mu\text{m}$ and $2.5 \mu\text{m}$, respectively.

As the plasmon frequency scales as inverse square-root of strip width (see (24)), in the latter case the plasmon resonance P_1 shifts to twice higher frequency than in the former case. It can be seen that the excitation of the plasmon mode adds to the radiation power (or Purcell factor) of antenna, however, at the expense of the spike in the absorption power. In the upper-THz range, the resonances on the WG modes appear, which are absent on the absorption plots because the rod is assumed lossless. A shift of the source from the rod plays little role.

The plots of the directivity of emission on panels (c) reveal very interesting interplay of three effects. One of them has GO nature – this is inverse EMJ effect, which is displayed as a remarkable steady growth of D with frequency from 1 in static limit to some 10 at 10 THz. The main lobe looks in the direction of $\phi = 180^\circ$. However, this growth is spoiled by the plasmon resonance P_1 , accompanied with a deep drop in the directivity. This is because the natural field of the first-order plasmon mode has the “dipole” pattern, with strong backward radiation (i.e. in the direction of $\phi = 0$). Note that, in the case of wider strip (Fig. 3(c)), this happens to be enough to “over-keel” the main lobe direction. If the strip is narrower (Fig. 4(c)), the resonance

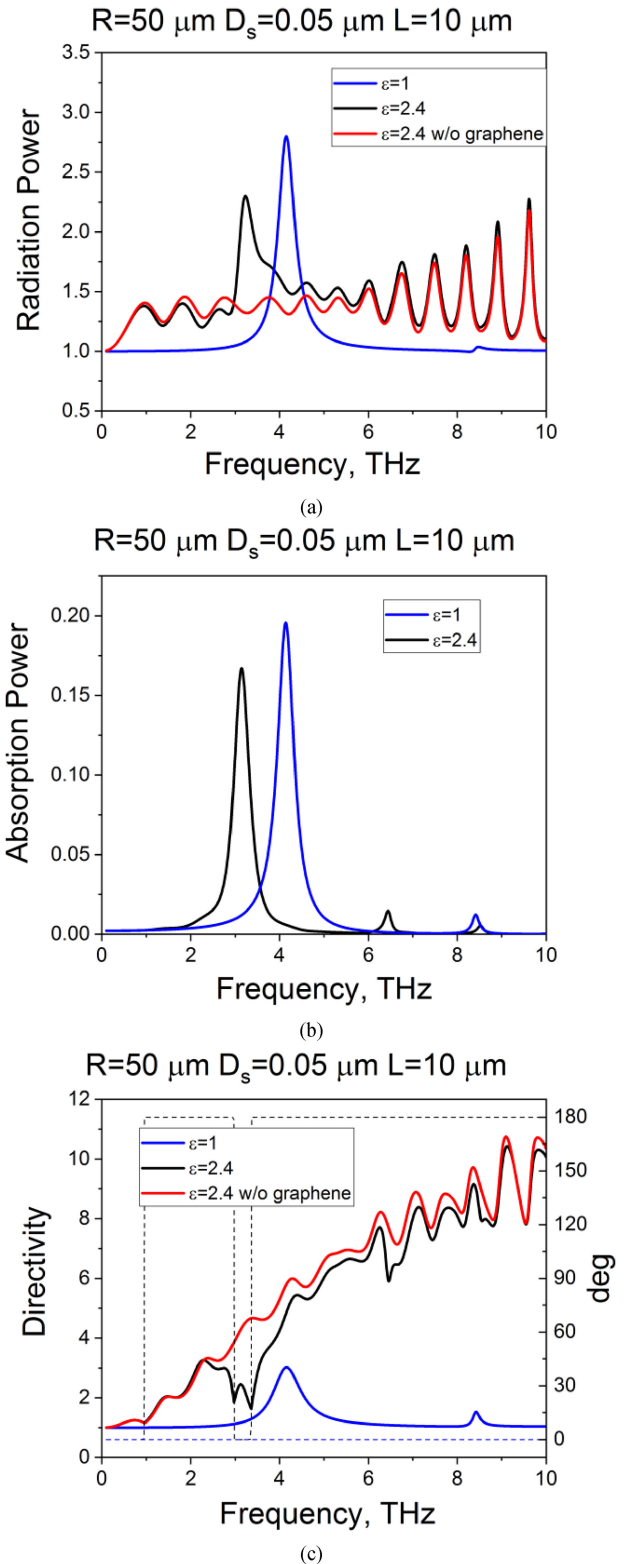
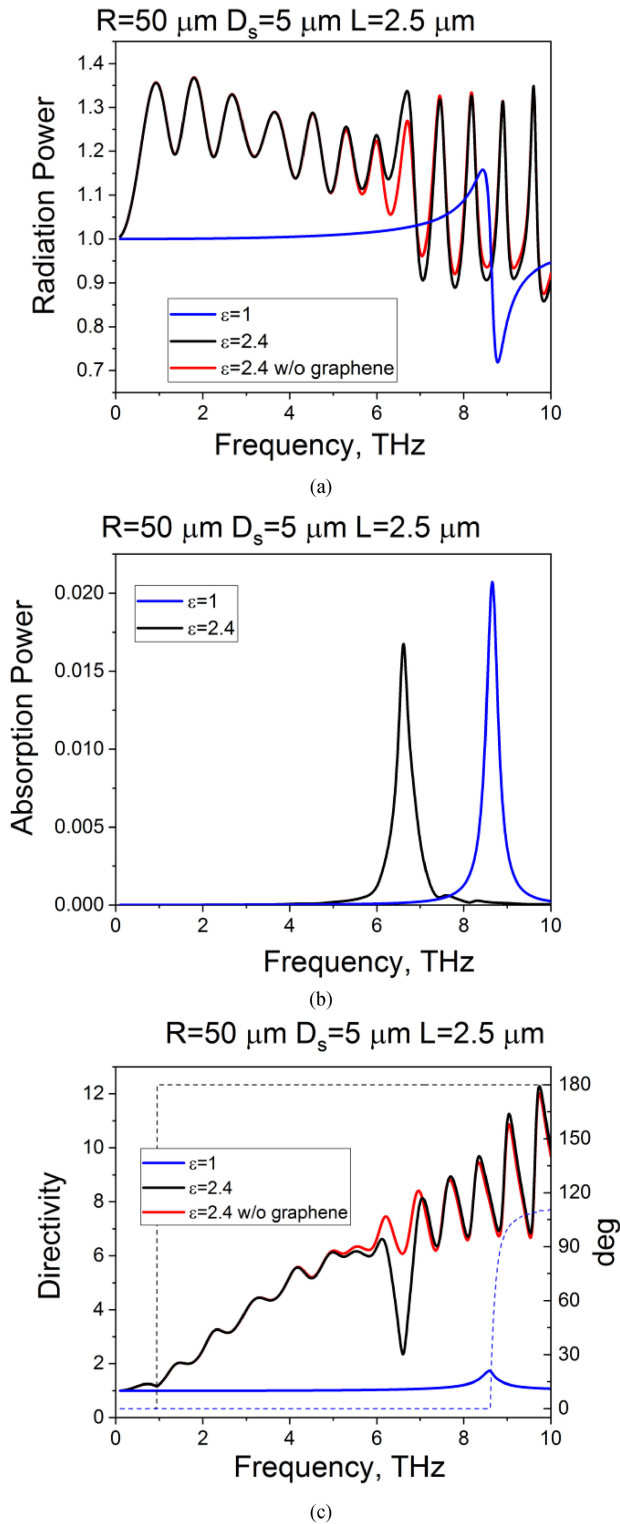
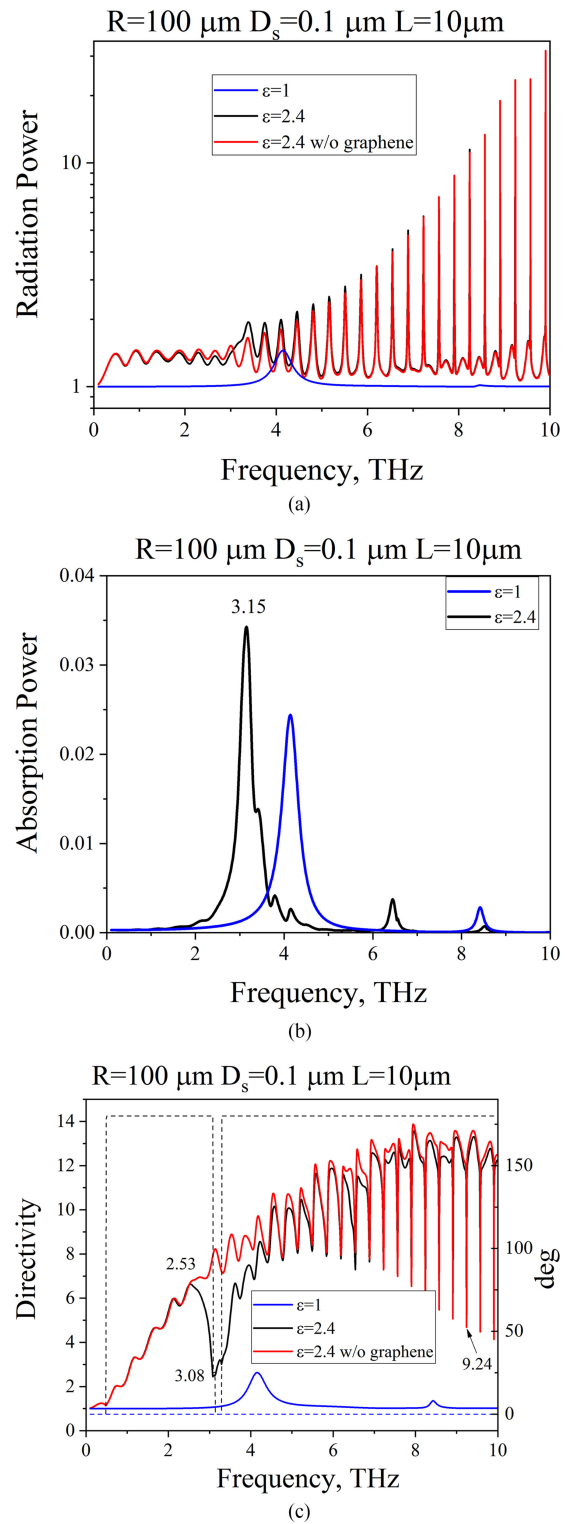


Fig. 3. Spectra of normalized radiation (a) and absorption power (b) and directivity (c) as a function of the frequency for the dielectric rod without graphene strip (red), with graphene strip (black), and for the graphene strip in the free space (blue). The dotted line on panel (c) depicts the main lobe radiation angle. Dielectric rod has radius of $R = 50 \mu\text{m}$ and permittivity $\varepsilon = 2.4$. Graphene width is $L = 10 \mu\text{m}$. The source is on the x -axis at the distance $D_s = 50 \text{ nm}$ from the rod.


 Fig. 4 Same in Fig. 3, however for $D_s = 5 \mu\text{m}$, $L = 2.5 \mu\text{m}$.

 Fig. 5 Same in Fig. 3, however for $R = 100 \mu\text{m}$, $D_s = 0.1 \mu\text{m}$.

P_1 appears at higher frequencies, where the inverse-EMJ effect is stronger, and then no resonance “over-keel” happens.

The plots in Fig. 5 show similar results, however for twice wider rod decorated with wide strip of graphene. In this case, the radiation power (i.e. the full-wave Purcell factor) displays

a periodic sequence of sharper and sharper spikes at higher frequencies. These are the resonances on the WG modes of the circular rod, H_{1m} ($m = 1, 2, \dots$), that have Q-factors, exponentially growing with azimuth index m . They are absent on the plots of the absorption power as the rod is assumed lossless.

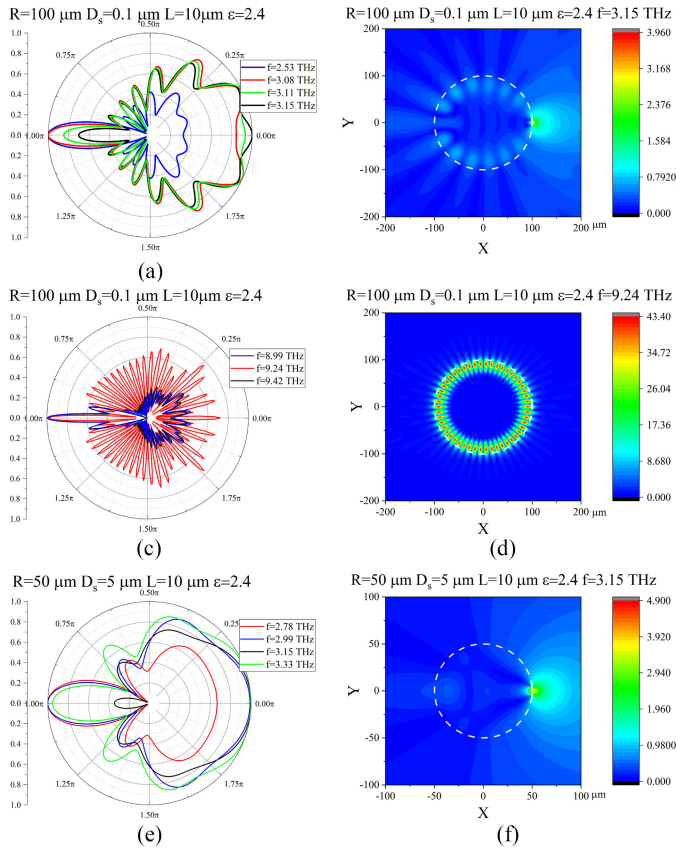


Fig. 6. Normalized far-field angular radiation patterns in and near to some of the peaks of absorption power in Figs. 3–5, and near field portraits in the peaks.

They spoil the directivity (i.e. the inverse-EMJ effect) in the same manner as the plasmon-mode resonance, although, unlike the latter, they cannot “over-keel” the main lobe.

To support our understanding of the behavior of the antenna directivity as a function of the frequency, we visualize, in Fig. 6, three sets of the normalized far-field radiation patterns and the near-field portraits. The former are plotted both in and off the resonances, and the latter are shown only in the resonances. In the case of plasmon resonance, they demonstrate enhanced backward radiation (a), (e) and near field, which sticks to the graphene strip (b), (f). The main lobe, in this resonance, looks in the backward direction.

In the case of the resonance on the WG-mode $H_{1,25}$, see panels (c) and (d), there are as many as 50 comparable lobes in the far-field pattern and 50 bright spots in the near field, inside the dielectric rod. Still, the main lobe of radiation looks in the forward direction even in the resonance.

Keeping in mind that even the best of available dielectric materials are lossy, we have also checked how these losses affect the above discussed antenna characteristics. In the language of the Purcell effect, this is equivalent to account of non-radiation decay rate due to both dielectric and graphene losses. The corresponding results are presented in Fig. 7 for the case of $\epsilon = 2.4 + i0.01$. They show that the plasmon-mode resonance

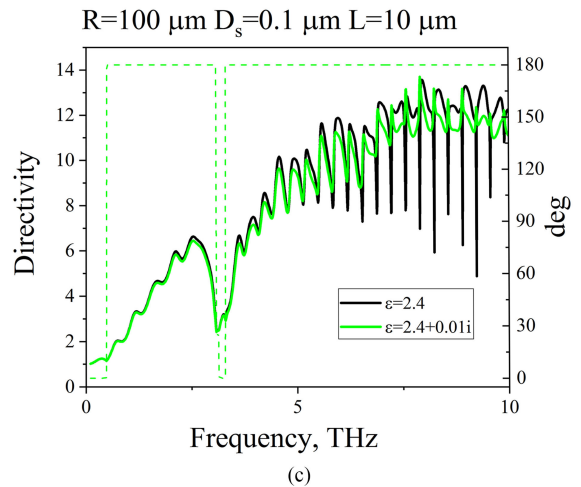
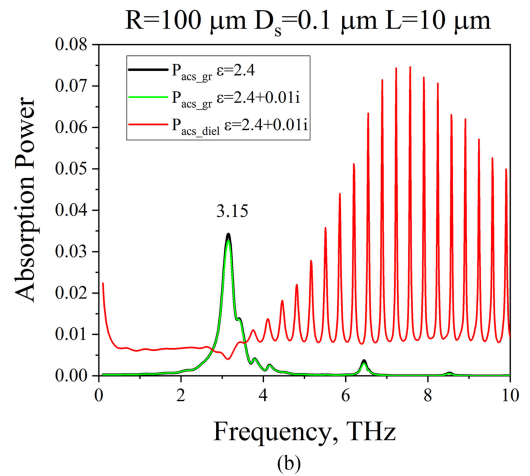
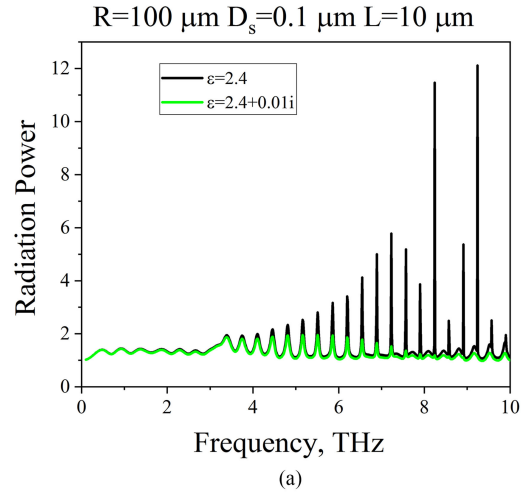


Fig. 7 Same characteristics as in Fig. 5, however for the lossy dielectric rod, $\epsilon = 2.4 + i0.01$. For comparison, the lossless rod data are also shown.

and associated drop in the directivity is almost intact. However, now the WG-modes appear as small but sharp spikes in the normalized absorption power. The plots of the radiation power and the directivity become smoother because the Q-factors of WG modes are now spoiled.

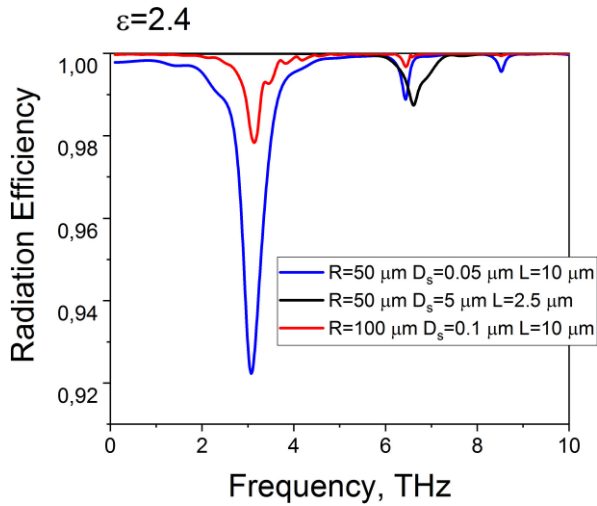


Fig. 8. Radiation efficiency as a function of frequency in the case of lossless dielectric rod. Antenna parameters are explained in the inset.

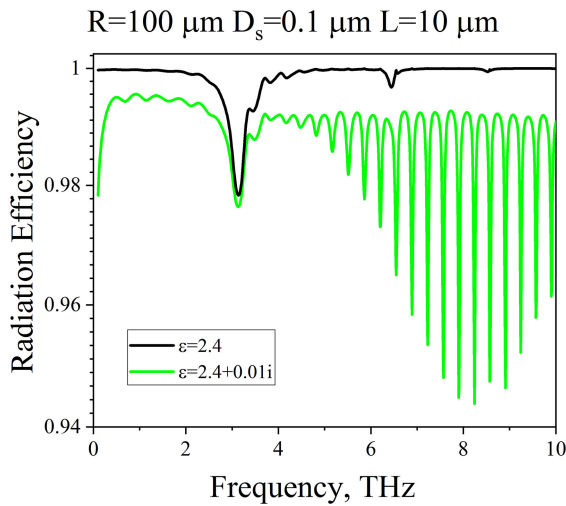


Fig. 9. Comparison of radiation efficiencies versus the frequency in the case of lossless (black) and lossy (green) dielectric rod.

Finally, we discuss the radiation efficiency of the studied photonic antenna. This is the same as quantum yield efficiency in terms of the Purcell effect. The frequency dependences of this quantity are presented in Figs. 8 and 9 for the lossless rod and lossy rod, respectively. As could be expected, the radiation efficiency drops in the plasmon resonances, however, this drop is only a few per cent as it has the order of $O(\text{Re}Z)$. In similar manner, if the rod is lossy then the efficiency drops in the WG-mode resonances; here the drops have the order of $O(\text{Im}\epsilon)$.

More complete understanding of the variation of the above discussed characteristics with frequency and strip size, for the other parameters taken as in Fig. 9, is provided by the color maps in Fig. 10. Here, one can easily discriminate between the WG-mode resonances, which have fixed frequencies, and plasmon-mode resonances, which follow equation (24).

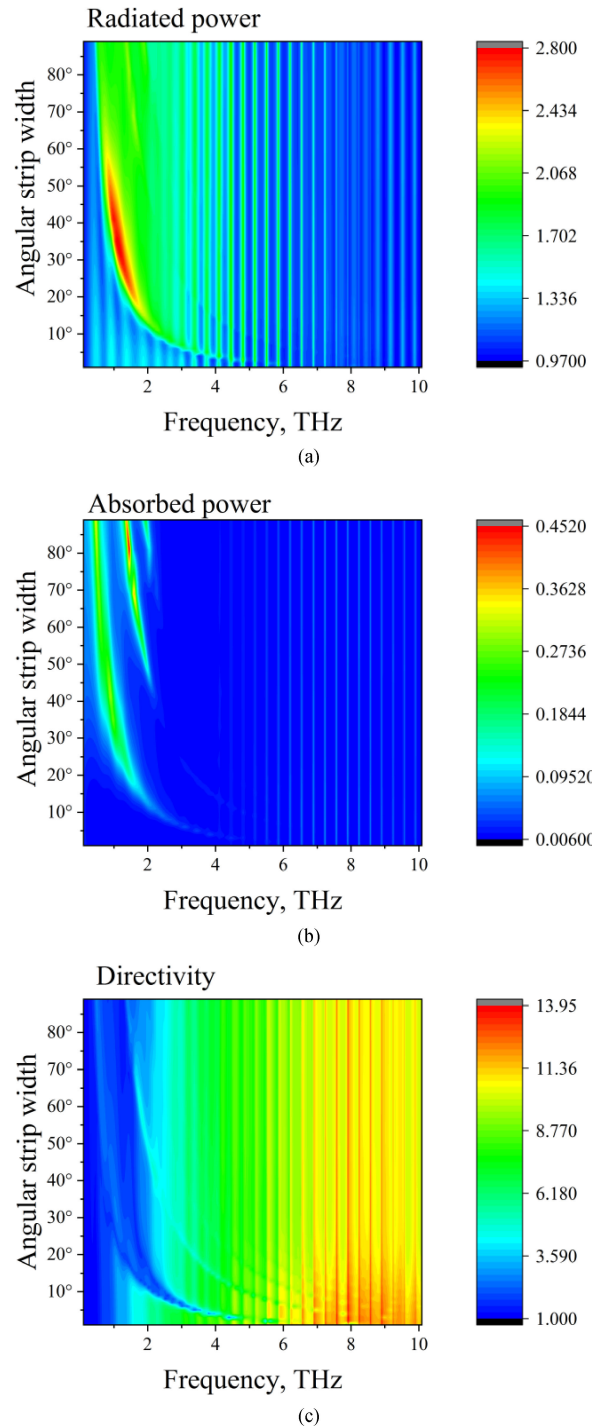


Fig. 10. Color maps of the normalized radiated (a) and absorbed (b) powers and the directivity (c) of emission versus the frequency and the strip angular width, for antenna with the other parameters being the same as in Fig. 9.

IV. CONCLUSION

We have presented the results of the accurate study of the modification of the H-polarized radiation emitted by magnetic line current, due to isotropic circular dielectric rod decorated with graphene strip. Our results, obtained by a mathematically grounded in-house algorithm based on judicious solution of the

hypersingular integral equation, have shown that such antenna is able to produce well-collimated radiation in the far zone, due to the inverse EMJ effect. However, this broadband collimation is spoiled if the frequency hits one of the natural frequencies, which are of two kinds: of the medium-Q strip-plasmon modes and of the extremely high-Q rod WG modes.

What appears to be important for applications, only the plasmon-mode resonances are tunable with the aid of DC bias, which changes the chemical potential of graphene. This makes possible electrically controlled binary operation of antenna at a fixed frequency, via the main lobe blinking in the forward direction. Note that if the strip were a PEC one, then the plasmon modes and the associated resonances would be absent.

REFERENCES

- [1] B. S. Lukyanchuk, R. Paniagua-Domínguez, I. Minin, O. Minin, and Z. Wang, "Refractive index less than two: Photonic nanojets yesterday, today and tomorrow," *Opt. Mat. Exp.*, vol. 7, no. 6, pp. 1820–1847, 2017.
- [2] A. Heifetz *et al.*, "Photonic nanojets," *J. Comput. Theor. Nanosci.*, vol. 6, no. 9, pp. 1979–1992, 2009.
- [3] R. K. Luneburg, *The Mathematical Theory of Optics*. Providence, RI, USA: Brown Univ. Press, 1941.
- [4] J. A. Lock, "Scattering of an electromagnetic plane wave by a Luneburg lens. III. Finely stratified sphere model," *J. Opt. Soc. Amer. A*, vol. 25, no. 12, pp. 2991–3000, 2008.
- [5] A. V. Boriskin and A. I. Nosich, "Whispering-gallery and Luneburg lens effects in a beam-fed circularly-layered dielectric cylinder," *IEEE Trans. Antennas Propagat.*, vol. 50, no. 9, pp. 1245–1249, Sep. 2002.
- [6] G. L. Hower, R. G. Olsen, D. J. Earls, and J. B. Schneider, "Inaccuracies in numerical calculation of scattering near natural frequencies of penetrable objects," *IEEE Trans. Antennas Propagat.*, vol. 41, no. 7, pp. 982–986, Jul. 1993.
- [7] A. V. Boriskin, S. V. Boriskina, A. Rolland, R. Sauleau, and A. I. Nosich, "Test of the FDTD accuracy in the analysis of the scattering resonances associated with high-Q whispering-gallery modes of a circular cylinder," *J. Opt. Soc. Amer. A*, vol. 25, no. 5, pp. 1169–1173, 2008.
- [8] J. Niegemann, W. Pernice, and K. Busch, "Simulation of optical resonators using DGTd and FDTD," *J. Opt. A, Pure Appl. Opt.*, vol. 11, no. 11, 2009, Art. no. 114015/10.
- [9] G. W. Hanson, "Dyadic Green's functions and guided surface waves for a surface conductivity model of graphene," *J. Appl. Phys.*, vol. 103, 2008, Art. no. 064302.
- [10] M. Jablan, H. Buljan, and M. Soljacic, "Plasmonics in graphene at infrared frequencies," *Phys. Rev. B*, vol. 80, 2009, Art. no. 245435.
- [11] M. Yasir and P. Savi, "Commercial graphene nanoplatelets-based tunable attenuator," *Electron. Lett.*, vol. 56, no. 4, pp. 184–187, 2020.
- [12] O. V. Shapoval and A. I. Nosich, "Bulk refractive-index sensitivities of the THz-range plasmon resonances on a micro-size graphene strip," *J. Phys. D: Appl. Phys.*, vol. 49, no. 5, 2016, Art. no. 055105/8.
- [13] A. P. Anyutin, I. P. Korshunov, and A. D. Shatrov, "Quasi-static plasmon resonances in a graphene ribbon in the infrared range," *J. Commun. Technol. Electron.*, vol. 61, no. 6, pp. 607–613, 2016.
- [14] W. Fuscaldo, P. Burghignoli, P. Baccarelli, and A. Galli, "Efficient 2-D leaky-wave antenna configurations based on graphene metasurfaces," *Int. J. Microw. Wireless Technol.*, vol. 9, no. 6, pp. 1293–1303, 2017.
- [15] O. V. Shapoval, J. S. Gomez-Diaz, J. Perruisseau-Carrier, J. R. Mosig, and A. I. Nosich, "Integral equation analysis of plane wave scattering by coplanar graphene-strip gratings in the THz range," *IEEE Trans. Terahertz Sci. Technol.*, vol. 3, no. 5, pp. 666–673, Sep. 2013.
- [16] S. V. Dukhopelnykov, R. Sauleau, M. Garcia-Vigueras, and A. I. Nosich, "Combined plasmon-resonance and photonic-jet effect in the THz wave scattering by dielectric rod decorated with graphene strip," *J. Appl. Phys.*, vol. 126, no. 2, 2019, Art. no. 023104.
- [17] M. V. Balaban, R. Sauleau, T. M. Benson, and A. I. Nosich, "Accurate quantification of the Purcell effect in the presence of a microdisk of nanoscale thickness," *Micro Nano Lett.*, vol. 6, no. 6, pp. 393–396, 2011.
- [18] A. E. Krasnok *et al.*, "An antenna model for the Purcell effect," *Sci. Rep.*, vol. 5, 2015, Art. no. 12956.
- [19] T. L. Zinenko, "Scattering and absorption of terahertz waves by a free-standing infinite grating of graphene strips: Analytical regularization analysis," *J. Opt.*, vol. 17, no. 5, 2015, Art. no. 055604/8.
- [20] M. E. Kaliberda, L. M. Lytvynenko, S. A. Pogarsky, and M. P. Roiuk, "Diffraction of the H-polarized plane wave by a finite layered graphene strip grating," *Int. J. Microw. Wireless Technol.*, vol. 11, pp. 1–8, 2019.
- [21] T. L. Zinenko, A. Matsushima, and A. I. Nosich, "Surface-plasmon, grating-mode and slab-mode resonances in THz wave scattering by a graphene strip grating embedded into a dielectric slab," *IEEE J. Sel. Top. Quant. Electron.*, vol. 23, no. 4, Jul./Aug. 2017, Art. no. 4601809.
- [22] M. Riso, M. Cuevas, and R. A. Depine, "Tunable plasmonic enhancement of light scattering and absorption in graphene-coated subwavelength wires," *J. Opt.*, vol. 17, 2015, Art. no. 075001/8.
- [23] E. A. Velichko, "Evaluation of a dielectric microtube with a graphene cover as a refractive-index sensor in the THz range," *J. Opt.*, vol. 18, no. 3, 2016, Art. no. 035008/11.
- [24] M. Naserpour *et al.*, "Tunable invisibility cloaking by using isolated graphene-coated nanowires and dimers," *Sci. Rep.*, vol. 12, 2017, Art. no. 12186/14.
- [25] T. Oguzer, A. Altintas, and A. I. Nosich, "Focusing of THz waves with a microsize cylindrical reflector made of graphene in the free space," *J. Eur. Opt. Soc.*, vol. 13, 2017, Art. no. 16.
- [26] Y. V. Gandel, "Parametric representations of integral and pseudo-differential operators in diffraction problems," in *Proc. Int. Conf. Mathem. Methods Electromag. Theory*, 2004, pp. 57–62.
- [27] A. S. Kononenko *et al.*, "Singular and hypersingular integral equations techniques for gyrotron coaxial resonators with a corrugated insert," *Int. J. Infrared Millimeter Waves*, vol. 28, no. 4, pp. 267–274, 2007.
- [28] A. V. Kostenko, "Numerical method for the solution of a hypersingular integral equation of second kind," *Ukrainian Mathem. J.*, vol. 65, no. 9, pp. 1373–1383, 2014.



Sergii V. Dukhopelnykov (Member, IEEE) was born in Kharkiv, Ukraine, in 1982. He received the B.S., M.S., and Ph.D. degrees in mathematical modeling and numerical methods from the Kharkiv National University, Kharkiv, Ukraine, in 2003, 2004, and 2010, respectively.

From 2007 to 2018, he was a Lecturer, Senior Lecturer, and Assistant Professor with the Department of Mathematics, National Technical University "Kharkiv Polytechnic Institute," Kharkiv, Ukraine.

Since 2018, he has been a Senior Scientist with the Laboratory of Micro and Nano Optics, Institute of Radio-Physics and Electronics, National Academy of Sciences of Ukraine, Kharkiv, Ukraine, and a part-time Assistant Professor with the School of Mathematics, Kharkiv National University. His research interests include singular integral equations, Nystrom methods, and patterned graphene scattering. Dr. Dukhopelnykov was a recipient of the Ph.D. Scholarship Award of the N. I. Akhizyzer Foundation, Kharkiv, Ukraine, in 2010 and the Young Scientist Prize of the International Conference on Mathematical Methods in Electromagnetic Theory in 2018.



Mario Lucido (Senior Member, IEEE) was born in Naples, Italy, in 1972. He received the Laurea degree in electronic engineering from the University of Napoli "Federico II," Naples, Italy, in 2000, and the Ph.D. degree in electrical and telecommunication engineering from the University of Cassino and Southern Lazio, Cassino, Italy, in 2004.

Since April 2005, he has been a Researcher with the University of Cassino and Southern Lazio, where he has been an Adjunct Professor of antennas and microwaves since 2006. He has authored about 80 scientific journal articles and conference papers. His research interests include semi-analytical techniques for the analysis of scattering problems, waveguide and optical waveguide propagation, microwave circuits, and microstrip antennas. Dr. Lucido is currently a member of the Italian Society of Electromagnetism, the National Inter-University Consortium for Telecommunications, ELEDIA Research Center, and the National Interuniversity Research Center on Interactions between Electromagnetic Fields and Biosystems. He was a recipient of the "Giorgio Barzilai" Prize for the Best Young Scientist Paper at the Italian National Congress on Electromagnetics in 2006 and the Volodymyr G. Sologub Senior Researcher Award for contribution to computational electromagnetics at the International Conference on Mathematical Methods in Electromagnetic Theory in Lviv in 2016.